



## Organofacies and paleoenvironment of lower Carboniferous mudstones (Dishuiquan Formation) in Eastern Junggar, NW China

Shengyin Zhang <sup>a</sup>, Tao Wu <sup>b</sup>, Shuncun Zhang <sup>a,\*</sup>, Chunhui Cao <sup>a</sup>, Wanyun Ma <sup>b</sup>, Ji'an Shi <sup>a</sup>, Guoqiang Sun <sup>a</sup>

<sup>a</sup> Key Laboratory of Petroleum Resources, Gansu Province/Key Laboratory of Petroleum Resources Research, Institute of Geology and Geophysics, Chinese Academy of Sciences, Lanzhou 730000, China

<sup>b</sup> Xinjiang Oilfield Company, PetroChina, Karamay, Xinjiang 834000, China



### ARTICLE INFO

#### Article history:

Received 20 January 2015

Received in revised form 28 June 2015

Accepted 6 August 2015

Available online 8 August 2015

#### Keywords:

Organic matter source

Biomarkers

Paleoenvironment

Paleoclimate

Lower Carboniferous mudstones

Eastern Junggar

### ABSTRACT

The sedimentary rocks of the Dishuiquan Formation represent an important potential source for volcanic rock reservoirs and record the transition of the depositional environment from marine to terrestrial during paleo-Junggar oceanic subduction. The source rock potential and paleoenvironment of mudstones from Dishuiquan Formation in Eastern Junggar, were determined by organic petrography, Rock-Eval, molecular and stable carbon ( $\delta^{13}\text{C}$ ) analyses. TOC, S<sub>2</sub>, and hydrogen index (HI) values suggest a fair to good organic richness in mudstone samples from the C-2 well. Moreover, an early mature to mature state for all the samples is inferred based on the Rock-Eval and biomarker parameters. The maceral composition, molecular geochemistry and carbon isotopic results for kerogen reveal that all the mudstone samples are characterized by a mixed organic matter assemblage (Types II–III) with relatively high percentages of terrigenous organic matter. The low to intermediate values of Pr/Ph and the high abundances of  $\beta$ -carotene and gammacerane indicate the presence of a dysoxic, reducing, high-salinity sedimentary environment during the deposition of the Dishuiquan Formation. Numerous parameters derived from the organic geochemical analyses indicate that the terrigenous organic matter increased with decreasing salinity and oxidation in the sedimentary environment. This study concludes that a warm, wet climate provided a continuous fluvial input of terrigenous plant debris and fresh water. The organic geochemical data, combined with the tectonic setting, reveal a restricted, semi-closed marine depositional environment during the deposition of the Dishuiquan Formation in the early Carboniferous.

© 2015 Elsevier B.V. All rights reserved.

## 1. Introduction

The Eastern Junggar Basin is located between the Altaids, or the Central Asian Orogenic Belt (CAOB) (Cai et al., 2012; Wilhem et al., 2012; Xiao et al., 2010), and the Tian Shan Orogenic Belt. The basin contains a large accumulation of Paleozoic volcanic and clastic sedimentary rocks, which record the history of Paleo-Asian ocean closure and the accretionary orogenesis (He et al., 2010; Xiao et al., 2013). Numerous studies have examined the geochemistry and chronology of the volcanic rocks from the Eastern Junggar Basin and the CAOB, and a widely accepted model relates Paleo-Asian ocean subduction with continental accretion during the later Paleozoic, which is constrained by the timing of ocean closure, collision and post-collision volcanic events (Han et al., 2011; Li et al., 2014; Liu et al., 2013; Yang et al., 2012a). However, few data concerning the sedimentary facies and environmental evolution of the Carboniferous sedimentary rocks along the subduction of the Paleo-Asian Ocean are available due to the intense volcanic activity and differential uplift following the early Carboniferous.

Fortunately, a major petroleum system (i.e., the Kalameil gas field) with a Carboniferous volcanic reservoir was discovered in the Eastern Junggar Basin during the last decade (He et al., 2010; Zou et al., 2013). The organic matter (OM) in the sedimentary rock of the lower Carboniferous is believed to be an important source for the gas in these reservoirs (He et al., 2010; Wang et al., 2010; Zou et al., 2013). The sedimentary successions under thick volcanic strata, especially the organic rich mudstones, could provide a window to understand the paleoenvironment during the Carboniferous.

This study used Rock-Eval pyrolysis, organic petrography, molecular and stable carbon ( $\delta^{13}\text{C}$ ) analyses to determine the organofacies and paleoenvironment of the lower Carboniferous Dishuiquan Formation mudstones during the transition from marine to terrestrial environments in the Eastern Junggar Basin and to evaluate the hydrocarbon potential of these mudstones.

## 2. Geological setting

The Junggar Basin is located at the triple junction of the Kazakhstan, Siberia and Tarim Plates (Fig. 1a). This multicycle superimposed basin is filled with late Paleozoic marine sediments and Mesozoic-Cenozoic continental sediments (He et al., 2013; Li et al., 2014; Xiao et al., 2013). The

\* Corresponding author.

E-mail address: [zhangshuncun@126.com](mailto:zhangshuncun@126.com) (S. Zhang).

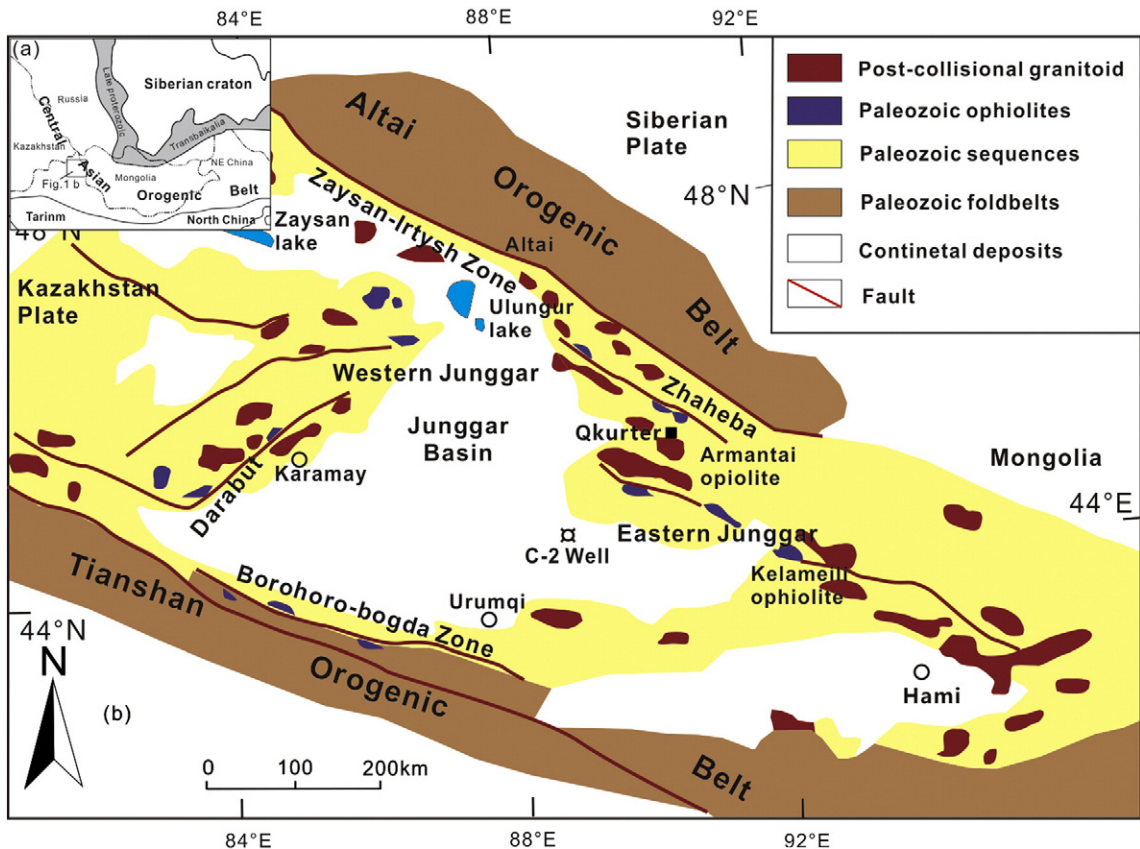


**Fig. 1.** (a) Location of northwestern China in the Central Asian Orogenic Belt, modified and simplified from Xiao and Santosh (2014). Panel b is outlined. (b) Simplified geological map surrounding Junggar Basin (Chen and Jahn, 2004), showing the C-2 well in Eastern Junggar.

basin is surrounded by Paleozoic orogens: the Tianshan Mountains to the south and the Altai Mountains to the north (Fig. 1b). The Eastern Junggar comprises the Eastern Junggar Basin and Eastern Junggar Terrane (Fig. 1b), which is part of the CAOB. The Eastern Junggar Terrane is characterized by several accretionary complexes related to subduction-accretion processes and was accreted to the southern margin of the Siberian block during the Paleozoic (Xiao and Santosh, 2014; Xu et al., 2013). Two NW-SE-trending, highly deformed and dismembered ophiolite belts, the northern Zhaheba-Aermantai and the southern Karamaili belts, crop out in the Eastern Junggar Terrane (Fig. 1b). Using U-Pb methods, the Zhaheba-Aermantai ophiolite belt was dated to  $489 \pm 4$ – $503 \pm 7$  Ma (Jian et al., 2003; Tang et al., 2007; Xiao et al., 2006; Zhang and Guo, 2010), whereas the Karamaili ophiolite belt has an early Devonian to early Carboniferous age based on SHRIMP zircon U-Pb methods (Su et al., 2012). The geochemical characteristics of the lower Carboniferous volcanic rocks reveal that early Carboniferous volcanism occurred in an island-arc setting related to the subduction of the Paleo-Junggar Ocean (Su et al., 2012; Xiao and Santosh, 2014; Yang et al., 2012a,b).

The Carboniferous in Eastern Junggar can be divided into four formations from base to top (Fig. 2). The Tamugang Formation consists of sedimentary tuff and basaltic tuff intercalated with marine sandstone. The Dishuiquan Formation comprises rhyolite, basaltic breccia, and andesite coarse clastic glutenite, topped with an approximately 400-m-thick mudstone. The Batamayineishan Formation consists of a 3300-m-thick succession of intermediate to basic volcanic rocks, including basalt, andesite, basaltic tuff and breccia, intercalated with sedimentary tuff and carbonaceous shale, which are considered to be rich in terrestrial organic matter. The Shiqiantan Formation is a suite of fine clastic rocks intercalated with intermediate mudstones (Yang et al., 2011, 2012c; Zhang et al., 2009). Furthermore, the Batamayineishan Formation and Shiqiantan Formation were denuded to varying degrees as a result of

differential uplift in Eastern Junggar during the late Carboniferous to late Permian.

The term "Dishuiquan Formation" previously only referred to a suite of dark mudstones in the Dishuiquan area to the east of Karamaili Mountain. This formation has also been drilled in the Ludong and Wucaiwian regions of the Junggar Basin in subsequent explorations and was thought to have great potential as a hydrocarbon source rock in the Carboniferous and post-Carboniferous periods. However, the suite of dark mudstones or similar mudstones also crops out in the lower Carboniferous Nanningshui Formation and Heishantou Formation in Eastern Junggar, and the Sunkarsu Formation includes a succession of coarse clastic andesitic glutenite, which is considered to be a coeval deposit developed on the proximal fan. In investigations of the depositional environment and source rock potential of the suite of dark mudstones, the Nanningshui Formation, Heishantou Formation, and Songkaersu Formation were grouped together as the lower Carboniferous Dishuiquan Formation (Tao et al., 2014; Wang et al., 2013).

### 3. Samples and methods

49 core samples were collected from a depth range of 3310–3732 m in the C-2 well located in the Wucaiwian area of Eastern Junggar (Fig. 1, Table 1). The sampled interval was within the Dishuiquan Formation, a lower Carboniferous mudstone, 20 samples of which were gray-green mudstone and the other 29 dark-gray mudstone. All collected samples were analyzed for total organic carbon (TOC) and Rock-Eval pyrolysis, and 10 samples were selected for maceral analysis of kerogen and stable carbon isotope analyses. In total, 42 samples were prepared for gas chromatography mass spectrometry (GC-MS) and chloroform bitumen "A" stable carbon isotope analysis.

The TOC was measured with a Leco CS-200 instrument. The crushed and sieved samples (approximately 100 mg, 120 mesh) were pre-

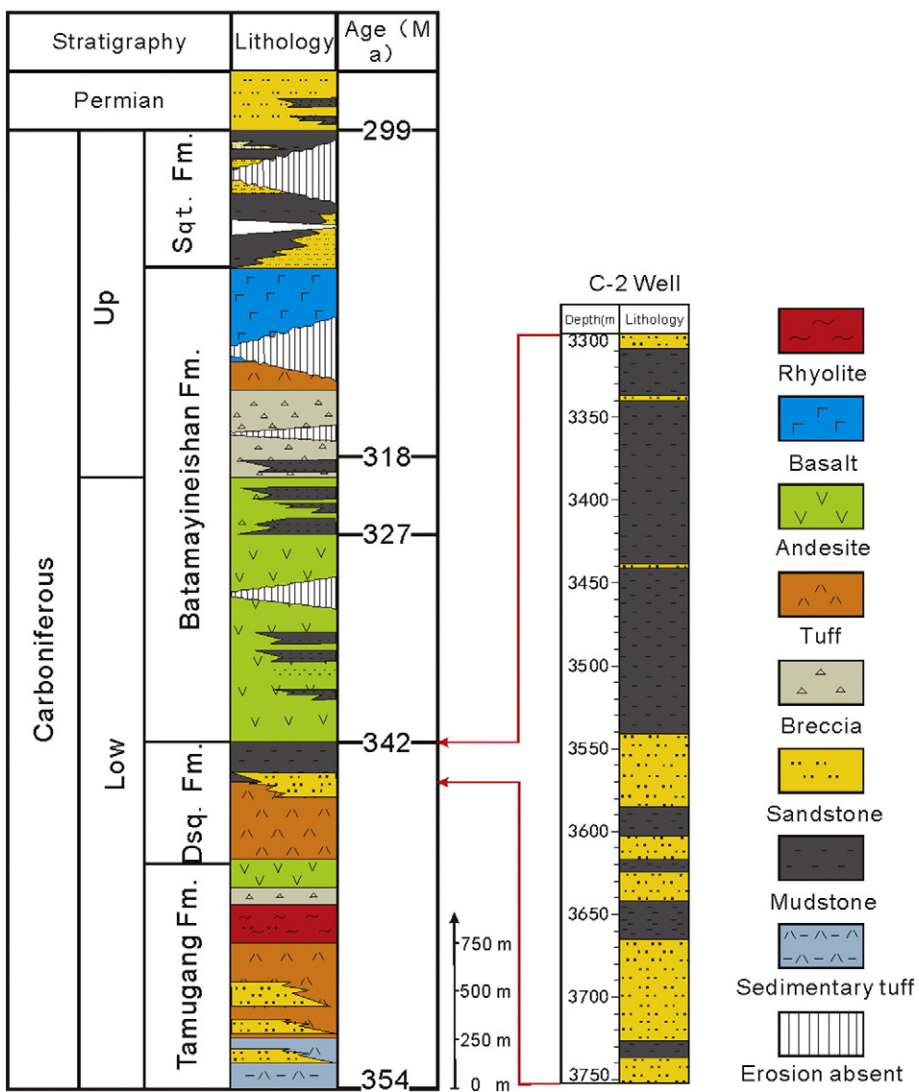


**Fig. 2.** Stratigraphic section through the Carboniferous in Eastern Junggar, showing the location of the samples from Dishuiquan Formation. "Dsq" and "Sqt" are the abbreviation of "Dishuiquan" and "Shiqiantan", respectively.

treated with 1 mol/L HCl to remove carbonate and then heated to 1200 °C in an induction furnace. The Rock-Eval pyrolysis data were collected using a Rock-Eval II instrument following guidelines established by Peter (1986) and Espitalié et al. (1986). The  $S_1$  signal represents any free hydrocarbons that can be volatilized out of the rock without cracking the kerogen (mg HC/g rock) at 300 °C. The  $S_2$  signal represents the amount of hydrocarbons (mg HC/g rock) that are expelled via kerogen cracking under temperature-specific pyrolysis (300–600 °C). The  $S_2$  peak represents the existing potential of a rock to generate petroleum if burial and maturation were to continue to completion. The  $S_1 + S_2$  parameter is a measurement of genetic potential, i.e., the total amount of petroleum that might be generated by a rock. The parameter  $T_{\max}$  (°C) is the Rock-Eval pyrolysis oven temperature at which the maximum pyrolytic liberation of hydrocarbons ( $S_2$ ) is observed and is indicative of thermal maturation (Hunt, 1996).

The powdered samples were extracted with chloroform in a Soxhlet apparatus for 72 h. The extracts (chloroform bitumen "A") were separated by column chromatography into saturated hydrocarbons, aromatic hydrocarbons, and NSO compounds using a silica gel alumina column after the precipitation of asphaltenes (Petersen et al., 2005). The GC for the saturated hydrocarbon fraction was performed on a HP6890 gas chromatograph fitted with a 30 m × 0.32 mm i.d. HP-5 column with a

film thickness of 0.25 μm and using nitrogen carrier gas. The oven temperature was initially set to increase from 80 °C to 320 °C at 10 °C/min and hold at 320 °C for 20 min. The GC-MS of saturated hydrocarbon fractions was performed on a Thermal Scientific DSQ II quadrupole mass spectrometer (fitted with a 30 m × 0.25 mm i.d. HP-5 MS column with a film thickness of 0.25 lm and using helium carrier gas). The oven was held for 1 min at 35 °C, then increased from 35 °C to 120 °C at 10 °C/min and from 120 °C to 300 °C at 3 °C/min, with a final holding time of 30 min at 300 °C. The selected ion-monitoring capabilities of the data-acquisition system permitted specific ions to be monitored, such as tricyclic terpanes and hopanes (m/z 191) and steranes (m/z 217) (Song et al., 2013).

To prepare the kerogen samples, fragments of rock were leached in 12 N HCl for 12 h to remove carbonates, then washed several times with distilled water and treated with hydrofluoric acid (HF) for 12 h to remove silicates. The samples were again washed several times with distilled water and again treated with 12 N HCl. Kerogen residues were mounted from distilled water onto coverslips which were then dried at 30–40 °C. Slides were then inverted onto coverslips with a drop of polyvinyl alcohol solution. The analysis was performed by reflected and transmitted white light and reflected UV fluorescence (Littke et al., 2012; Sachse et al., 2012; Wang et al., 2011).

**Table 1**

Results of Rock-Eval and TOC analysis and calculated parameters.

Sample no.	Lithology	Depth (m)	TOC (%)	$T_{\max}$ (°C)	$S_1$	$S_2$	HI	PI
					mg HC/g TOC			
CC-1	Gray-green mudstone	3310	0.3	u.r.	0.03	0.31	u.r.	0.09
CC-2	Gray-green mudstone	3315	0.6	u.r.	0.04	0.55	u.r.	0.07
CC-3	Gray-green mudstone	3320	0.7	433	0.05	0.67	97	0.06
CC-4	Gray-green mudstone	3325	1.0	440	0.06	1.23	127	0.05
CC-5	Gray-green mudstone	3330	0.9	441	0.06	1.03	121	0.05
CC-6	Gray-green mudstone	3335	0.6	430	0.07	0.87	136	0.08
CC-7	Gray-green mudstone	3340	0.8	433	0.1	1.09	140	0.09
CC-8	Gray-green mudstone	3345	1.0	434	0.12	1.15	121	0.1
CC-9	Gray-green mudstone	3350	1.0	436	0.13	1.13	109	0.1
CC-10	Gray-green mudstone	3355	1.1	439	0.08	1.12	101	0.07
CC-11	Gray-green mudstone	3360	0.8	440	0.07	0.92	110	0.07
CC-12	Gray-green mudstone	3365	1.0	439	0.09	1.2	117	0.07
CC-13	Gray-green mudstone	3370	1.1	441	0.11	1.48	140	0.07
CC-14	Gray-green mudstone	3375	1.2	441	0.11	1.54	128	0.07
CC-15	Gray-green mudstone	3380	1.3	443	0.11	1.85	143	0.06
CC-16	Dark-gray mudstone	3385	1.0	444	0.09	1.33	130	0.07
CC-17	Dark-gray mudstone	3391	1.0	441	0.13	1.35	136	0.08
CC-18	Dark-gray mudstone	3395	0.9	438	0.09	1	118	0.08
CC-19	Dark-gray mudstone	3400	0.8	440	0.09	0.99	118	0.08
CC-20	Dark-gray mudstone	3405	0.9	439	0.1	1.11	119	0.08
CC-21	Dark-gray mudstone	3410	0.9	440	0.09	1.09	117	0.08
CC-22	Dark-gray mudstone	3415	0.9	443	0.1	1.23	134	0.07
CC-23	Dark-gray mudstone	3420	0.8	440	0.08	1.01	125	0.07
CC-24	Dark-gray mudstone	3425	0.9	440	0.1	1.23	138	0.08
CC-25	Dark-gray mudstone	3430	0.9	446	0.07	1.04	118	0.06
CC-26	Dark-gray mudstone	3445	1.0	438	0.17	1.24	123	0.12
CC-27	Dark-gray mudstone	3450	0.7	439	0.07	0.81	109	0.08
CC-28	Dark-gray mudstone	3455	0.8	440	0.08	0.83	104	0.09
CC-29	Dark-gray mudstone	3459	0.6	438	0.07	0.64	105	0.1
CC-30	Dark-gray mudstone	3465	0.7	440	0.07	0.79	107	0.08
CC-31	Dark-gray mudstone	3470	0.8	431	0.11	0.8	105	0.12
CC-32	Dark-gray mudstone	3475	0.7	440	0.07	0.71	103	0.08
CC-33	Dark-gray mudstone	3480	0.7	435	0.08	0.77	105	0.1
CC-34	Dark-gray mudstone	3485	0.7	437	0.08	0.8	114	0.09
CC-35	Dark-gray mudstone	3490	0.7	426	0.13	0.83	119	0.13
CC-36	Dark-gray mudstone	3495	0.7	436	0.08	0.73	109	0.1
CC-37	Dark-gray mudstone	3505	0.6	440	0.06	0.71	111	0.08
CC-38	Dark-gray mudstone	3510	0.7	436	0.08	0.75	101	0.1
CC-39	Dark-gray mudstone	3515	0.5	u.r.	0.06	0.47	u.r.	0.12
CC-40	Dark-gray mudstone	3520	0.6	u.r.	0.07	0.55	u.r.	0.11
CC-41	Dark-gray mudstone	3525	0.6	u.r.	0.1	0.49	u.r.	0.16
CC-42	Dark-gray mudstone	3530	0.6	u.r.	0.1	0.56	u.r.	0.15
CC-43	Gray-green mudstone	3535	0.5	431	0.08	0.51	96	0.13
CC-44	Gray-green mudstone	3590	1.0	418	0.45	1.23	121	0.27
CC-45	Gray-green mudstone	3595	0.6	u.r.	0.14	0.54	u.r.	0.2
CC-46	Gray-green mudstone	3600	0.6	430	0.24	0.69	117	0.25
CC-47	Dark-gray mudstone	3660	0.3	u.r.	0.13	0.4	u.r.	0.25
CC-48	Dark-gray mudstone	3663	0.5	u.r.	0.14	0.35	u.r.	0.29
CC-49	Dark-gray mudstone	3732	1.0	445	0.14	1.27	132	0.1

u.r.: not reliable as the  $S_2 < 0.6$ .

The carbon isotopic values of the kerogen and chloroform bitumen "A" were determined with an EA-Finnigan Delta plus XL mass spectrometer. The results of the carbon isotope analysis are reported in the usual  $\delta$ -notation relative to the Pee Dee Belemnite (PDB) standard, and the analytical precision of this method was better than  $\pm 0.2\text{‰}$ . The reproducibility was better than 0.2% (Fu et al., 2009; Song et al., 2013).

## 4. Results

### 4.1. Bulk geochemical parameters

#### 4.1.1. TOC and Rock-Eval

The TOC values from samples CC-1 to CC-49 are in the range of 0.30–1.29% (Table 1), with an average of 0.79%. The Rock-Eval  $S_1$  and  $S_2$  values exhibit ranges of 0.03–0.45 and 0.31–1.85 mg HC/g rock, respectively. The production index (PI; PI =  $S_1$  / [ $S_1 + S_2$ ]) is in the range of 0.05–0.29. The  $T_{\max}$  values vary in the range of 418–446 °C ( $R_o$  ranged from 0.3% to 1.2%) (Fig. 3). The hydrogen index (HI) varies from 68 to

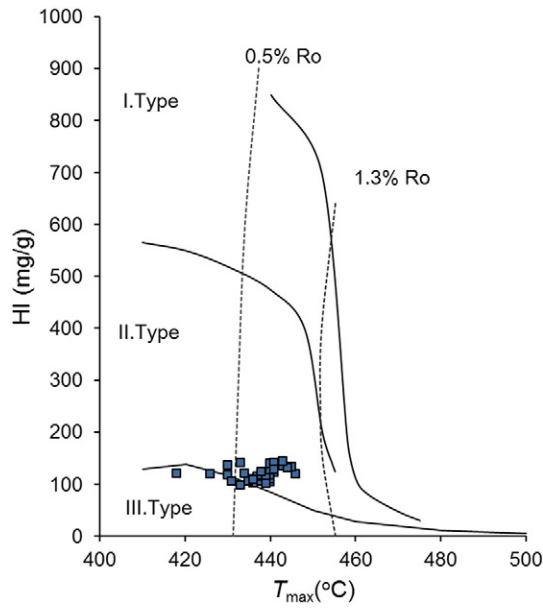


Fig. 3. Plot of HI vs.  $T_{\max}$  according to Espitalié et al. (1984) outlining kerogen type of Dishuiquan mudstones from C-2 well.

143 mg HC/g TOC, averaging 114 mg HC/g TOC. The average "true" HI of all samples from C-2, obtained according to the slope of the  $S_2$  vs. TOC regression line ( $R^2 = 0.93$ ), is 114.02 mg HC/g TOC (Langford and Blanc-Valleron, 1990).

#### 4.1.2. Maceral composition of kerogen

Amorphous sapropelic, amorphous humic, vitrinite, and inertinitite were detected in the 10 selected samples. The kerogen assemblages consist of 25–40% amorphous sapropelic OM, along with 31–50% amorphous humic OM, 7–12% vitrinite, and 9–27% inertinitite (Table 2).

### 4.2. Molecular geochemistry of organic matter

#### 4.2.1. n-Alkanes, acyclic isoprenoids and $\beta$ -carotane

The n-alkane and isoprenoid distributions were analyzed via gas chromatography. Table 3 summarizes the results for the carbon preference index (CPI<sub>15–23</sub> CPI<sub>25–35</sub>) (Bray and Evans, 1961) and other deterministic ratios of isoprenoids and n-alkanes. On the gas chromatogram of the samples from Dishuiquan Formation, a unimodal n-alkane distribution with a maximum at C15 or C19 is observed, and short-chain n-alkanes are more dominant than long-chain n-alkanes (Fig. 4). Certain samples at depths of 3460–3732 m have few or no C<sub>27+</sub> n-alkanes (Fig. 4, Table 3). The ratios of the short-chain to long-chain n-alkanes [ $\sum C_{21-} / \sum C_{22+}$ ] are in the range of 1.47–8.98, with an average of 3.72. The CPI<sub>1</sub> is defined as 1 / [2( $\sum C_{15-21}$  odd carbon) /  $\sum C_{14-20}$  even carbon] +  $\sum C_{15-21}$  odd carbon /

Table 2

Maceral composition and carbon isotope of kerogen form the Dishuiquan Formation mudstones.

Sample no.	Amorphous sapropelic OM	Amorphous humic OM	Vitrinite	Inertinitite	$\delta^{13}\text{C}$ (‰)
CC-2	31	49	9	11	-26.75
CC-5	31	50	10	9	-26.29
CC-9	32	49	8	11	-26.20
CC-12	31	48	9	12	-26.50
CC-15	25	44	12	19	-26.62
CC-18	34	41	8	17	-25.74
CC-20	31	31	11	27	-25.66
CC-21	33	43	8	16	-25.57
CC-41	40	35	7	18	-25.37
CC-48	34	45	8	13	-24.33

**Table 3**

n-Alkanes, acyclic isoprenoids, aromatic carotenoids parameters, and  $\delta^{13}\text{C}$  of chloroform extraction of samples from Dishuiquan Formation.

Sample no.	$C_{\max}$	$\text{CPI}_{15-23}$	$\text{CPI}_{25-35}$	$\text{Alk}_{\text{terr}}$	$\sum n\text{C}_{21-} / \sum n\text{C}_{22+}$	$\text{Pr/C}_{17}$	$\text{Ph/C}_{18}$	$\text{Pr/Ph}$	$\beta\text{-carotane}/\sum C_{12-35} (\%)$	$\delta^{13}\text{C CE}^{\text{a}}$
CC-2	C17	1.11	2.52	1.20	5.12	0.76	0.65	1.43	1.28	-28.50
CC-3	C17	1.08	2.10	2.26	3.49	0.76	0.63	1.32	1.89	-29.51
CC-4	C17	1.11	1.73	5.34	2.79	0.89	0.59	1.76	0.73	-29.19
CC-5	C17	1.10	2.27	4.86	3.33	0.70	0.55	1.55	1.37	-29.36
CC-9	C19	1.10	2.57	0.03	2.29	0.63	0.48	1.20	1.65	-29.57
CC-10	C17	1.11	1.75	4.80	3.28	0.74	0.64	1.40	1.19	-29.57
CC-11	C17	1.10	2.04	2.99	2.98	0.82	0.62	1.38	n.d.	-29.77
CC-12	C17	1.11	1.60	6.30	2.24	0.87	0.68	1.50	1.02	-29.69
CC-13	C17	1.12	1.62	4.81	2.37	0.81	0.63	1.45	1.09	-29.67
CC-14	C17	1.12	1.65	6.29	2.32	0.84	0.63	1.55	2.26	-29.44
CC-15	C17	1.10	1.62	9.12	1.47	0.81	0.57	1.51	1.04	-29.41
CC-16	C17	1.12	1.74	3.30	3.51	0.65	0.56	1.39	1.65	-29.29
CC-17	C19	1.08	2.16	3.71	2.50	0.65	0.58	1.08	2.74	-29.52
CC-18	C17	1.12	2.00	5.56	2.25	0.69	0.57	1.27	2.27	-29.24
CC-19	C16	1.10	1.95	3.03	3.68	0.62	0.53	1.57	2.28	-29.02
CC-20	C17	1.12	1.94	3.77	3.09	0.65	0.56	1.45	3.64	-29.26
CC-21	C17	1.09	1.82	4.00	2.50	0.64	0.50	1.40	n.d.	-29.24
CC-22	C17	1.07	2.25	5.45	2.93	0.61	0.57	1.29	n.d.	-29.10
CC-23	C19	1.09	1.23	6.37	1.80	0.70	0.60	1.12	2.26	-29.24
CC-24	C19	1.10	1.57	3.02	2.12	0.67	0.58	1.06	3.30	-29.00
CC-25	C17	1.11	1.63	3.83	2.50	0.64	0.55	1.28	n.d.	-28.67
CC-26	C17	1.05	2.01	0.00	5.31	0.62	0.59	1.15	4.27	-29.49
CC-27	C17	1.09	n.d.	0.00	5.65	0.61	0.59	1.05	3.54	-29.42
CC-28	C17	1.09	2.61	1.32	4.42	0.70	0.57	1.33	2.23	-29.08
CC-29	C17	1.08	2.42	0.00	5.09	0.66	0.62	1.09	3.11	-29.37
CC-30	C19	1.05	1.55	2.91	2.82	0.60	0.57	0.81	3.22	-29.30
CC-31	C17	1.08	n.d.	0.00	7.27	0.63	0.62	1.29	2.27	-29.38
CC-32	C21	1.14	1.66	5.69	1.66	0.62	0.59	1.07	1.96	-29.55
CC-33	C17	1.10	3.12	1.60	5.78	0.60	0.59	1.21	1.96	-29.22
CC-34	C17	1.10	3.12	1.60	5.78	0.60	0.59	1.21	1.96	-29.47
CC-35	C19	1.06	n.d.	0.00	4.52	0.65	0.60	0.91	4.31	-32.71
CC-36	C17	1.08	n.d.	0.00	8.99	0.58	0.57	1.24	2.05	-29.27
CC-37	C16	1.11	2.63	3.53	2.58	0.59	0.50	1.54	1.77	-29.27
CC-38	C16	1.11	2.37	1.03	6.10	0.55	0.52	1.35	1.65	-29.07
CC-40	C17	1.07	n.d.	0.00	5.33	0.62	0.60	1.09	3.30	-29.39
CC-41	C17	1.06	n.d.	0.00	6.80	0.59	0.55	1.22	3.59	-29.38
CC-42	C19	1.08	1.33	0.00	2.44	0.65	0.61	1.01	n.d.	-29.63
CC-43	C25	0.94	1.19	0.00	2.30	0.52	0.51	1.07	n.d.	-29.26
CC-44	C19	1.06	n.d.	0.00	6.16	0.51	0.48	0.99	1.73	-29.75
CC-45	C19	1.06	n.d.	0.00	3.58	0.54	0.53	0.77	2.27	-29.44
CC-46	C19	1.06	n.d.	0.00	4.12	0.60	0.54	0.91	3.12	-29.55
CC-48	C19	1.05	n.d.	0.00	4.70	0.46	0.47	0.82	4.48	-29.57
CC-49	C19	1.07	1.39	4.69	2.25	0.59	0.41	1.41	1.13	-29.16

n.d.: not detected.

<sup>a</sup>  $\delta^{13}\text{C CE} = \delta^{13}\text{C}$  of chloroform extraction.

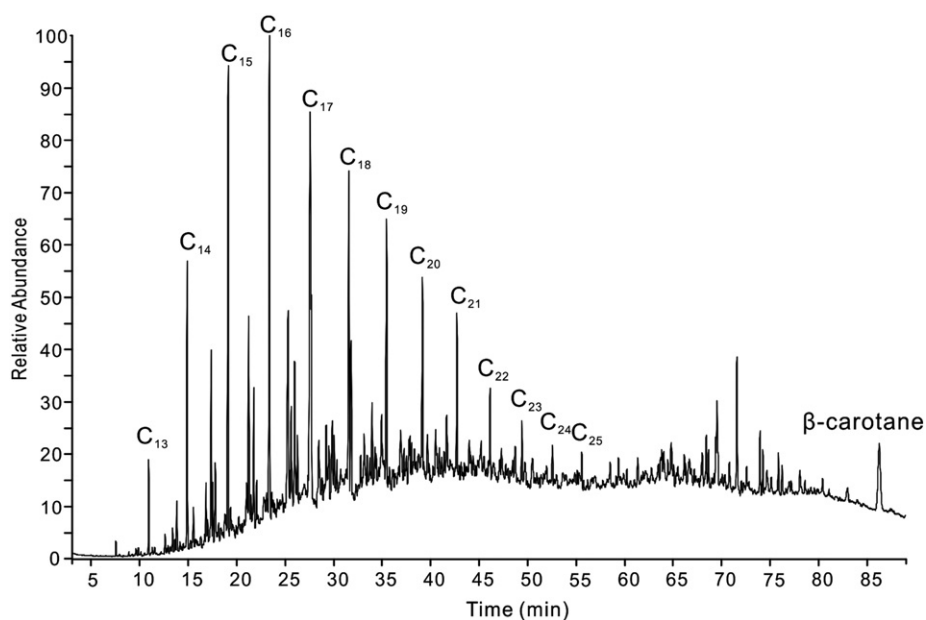


**Fig. 4.** Gas chromatograms (TIC) of saturated hydrocarbon fraction of mudstone (CC-10) of the Dishuiquan Formation.

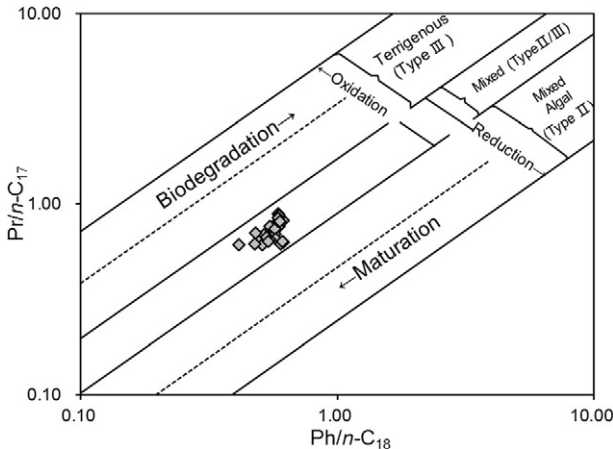


**Fig. 5.** Cross-correlation of pristane/n-C<sub>17</sub> versus phytane/n-C<sub>18</sub> ratios (Connan and Cassou, 1980).

$\sum C_{16-22}(\text{even carbon})$ ], and the CPI<sub>2</sub> is defined as  $1/2[\sum C_{25-35}(\text{odd carbon})/\sum C_{24-34}(\text{even carbon}) + \sum C_{25-35}(\text{odd carbon})/\sum C_{26-36}(\text{even carbon})]$ . The values of CPI<sub>1</sub> and CPI<sub>2</sub> are 0.94–1.36 and n.d.–3.12, respectively, which indicate that odd-numbered n-alkanes are dominant over even-numbered n-alkanes. The sum of the most abundant n-alkanes related to biogenic terrestrial sources (C<sub>27</sub>, C<sub>29</sub>, C<sub>31</sub>, C<sub>33</sub>) is referred to here as Alkterr and features values of n.d.–9.12% of the total n-alkanes in the samples from the C-2 well.

The acyclic isoprenoid pristane (Pr) and phytane (Ph) are present in considerable abundance in all samples. The Pr/C<sub>17</sub> and Ph/C<sub>18</sub> ratios are 0.46–0.89 and 0.41–0.68, respectively. The ratio of Pr to Ph in the samples ranges from 0.77 to 1.76, with an average of 1.24 (Figs. 4 and 5, Table 3). The compound β-carotane is present in considerable quantity in most samples (Fig. 4). The ratio of β-carotane and the sum of n-

alkanes ( $\beta\text{-carotane}/\sum C_{12-35}$ ) is in the range of n.d.–4.48%, and the values decrease upward (Fig. 6, Table 3).

#### 4.2.2. Hopanoids and steranes

Terpanes (including hopanoids) are important non-aromatic cyclic triterpenoid components of the lower Carboniferous mudstone in the Eastern Junggar. On the m/z 191 terpane fragmentograms of the C-2 well samples, tricyclic terpanes are observed in low abundance; the most abundant of these low-abundance terpanes C<sub>21</sub>- or C<sub>23</sub>-tricyclic terpanes (Fig. 7a). The hopanoid patterns are characterized by 17α,21β(H)- and 17β,21α(H)-hopanes from C<sub>27</sub> to C<sub>35</sub>, with an absence of C<sub>28</sub> hopanes and a predominance of 17α,21β(H)-C<sub>30</sub> hopanes. The ratio of 22S/(22S + 22R) for the 17β,21α(H)-C<sub>31</sub> hopanes is in the range of 0.54–0.58 (Table 4), whereas the average of 22S/(22S + 22R) for the 17β,21α(H)-C<sub>32</sub> hopanes is 0.59. The C-2 samples exhibit averages of 0.49 and 0.52 for C<sub>35</sub>/C<sub>34</sub> and C<sub>29</sub>/C<sub>30</sub>, respectively.

Gammacerane was detected in all the samples from the C-2 well in Eastern Junggar. The gammacerane index calculated from the ratio of 2 × gammacerane/(S + R)-C<sub>30</sub> hopanes is in the range of 0.62 to 1.89 (Table 4), and the values decrease upward. The values of Ts and Tm were also measured using the ion trace of m/z 191. The compound 18 α(H)-22,29,30-trisnorhopane (Ts) is generally considered to be more thermally stable than 17 α(H)-22,29,30-trisnorhopane (Tm). The Ts/Tm values range from 0.62 to 1.98, a range similar to the gammacerane index ( $R^2 = 0.58$ ) (Fig. 8).

Steranes are abundant in all of the samples (Table 5). The 5α,14α,17α(H) steranes, dominated by the 5α,14α,17α(H) isomers, are present in the C<sub>27</sub>–C<sub>29</sub> range (Fig. 7b). The 5α,14α,17α(H)20R isomer distributions of regular steranes in the samples from the upper part and lower part of the C-2 well are C<sub>29</sub> > C<sub>27</sub> > C<sub>28</sub> and C<sub>29</sub> > C<sub>28</sub> > C<sub>27</sub>, respectively. All the samples show a lower proportion of C<sub>27</sub> steranes compared to C<sub>29</sub> steranes among the C<sub>27</sub>–C<sub>29</sub> 5α,14α,17α(H)20R isomers. Additionally, the mudstone samples

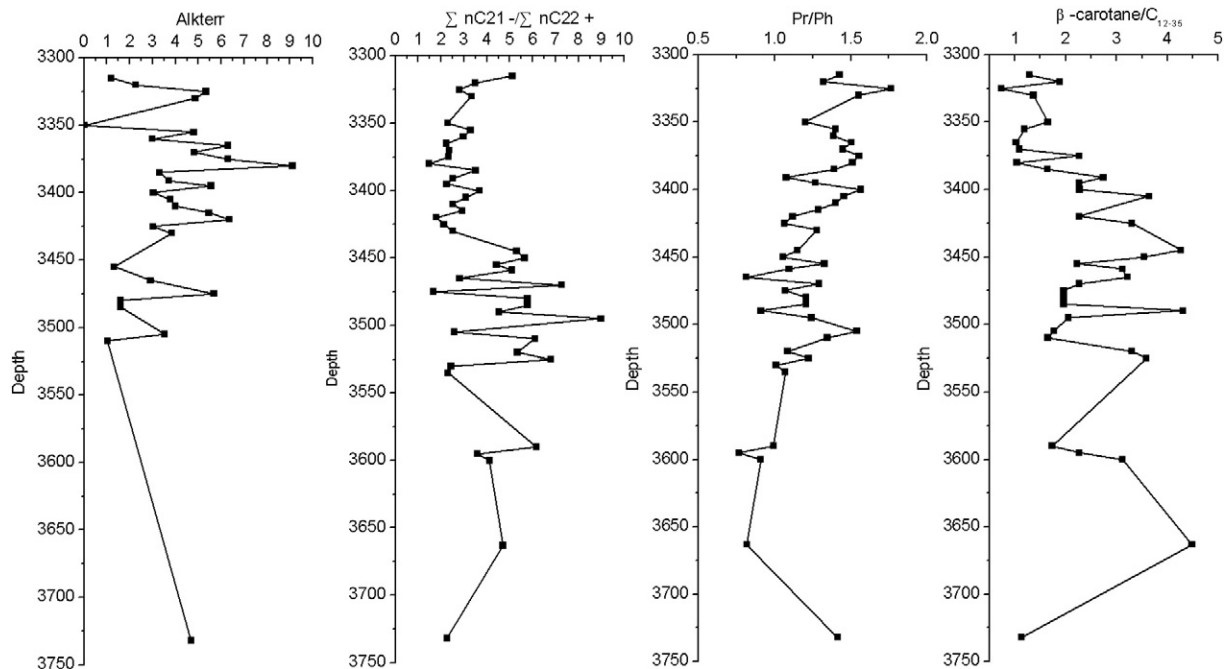


**Fig. 6.** Profile for parameters from n-Alkanes, acyclic isoprenoids, aromatic carotenoids of samples from Dishuiquan Formation, showing the negative relationship between the value of  $\beta\text{-carotane}/\sum C_{12-35}$  and Pr/Ph.

from C-2 well exhibit averages of 0.42 and 0.41 for  $C_{29}\alpha\alpha\alpha$ -20S/(20S + 20R) and  $C_{29}\alpha\beta\beta$ /( $\alpha\beta\beta$  +  $\alpha\alpha\alpha$ ), respectively.

#### 4.2.3. $\delta^{13}C$ values of kerogen and chloroform extract

The kerogen  $\delta^{13}C$  values for the Dishuiquan Formation vary in the range of  $-26.75\text{‰}$  to  $-24.33\text{‰}$ , with an average of  $-25.90\text{‰}$  (Table 2). The chloroform extracts from the C-2 well mudstones have lower stable carbon isotope values that range from  $-32.71\text{‰}$  to  $-28.50\text{‰}$ .

## 5. Discussion

### 5.1. Petroleum potential and maturity

The TOC values from the mudstones in the Eastern Junggar indicate that the mudstone is a fair to good petroleum source rock according to evaluation criteria of organic matter abundance of argillaceous source rocks established by the China National Petroleum Corporation in the 1990s (Han et al., 2014). However, based on the S2 values, which represent the fraction of the organic matter that can be transformed into hydrocarbons via high temperature, most of the mudstone samples show a fair source rock character. The samples from the C-2 well match the field characteristics of Type II–III kerogen in the HI vs.  $T_{max}$  diagram (Fig. 3)

(Espitalié et al., 1984). Based on the data above, it can be easily concluded that the organic matter in the mudstones is capable of generating oil and gas in the Dishuiquan Formation.

The production index (PI;  $PI = S_1/[S_1 + S_2]$ ) reaches approximately 0.4 at the bottom of the oil window and less than 0.1 at the top of the oil window (Peter, 1986). The PI for the mudstone samples is in the range of 0.05 to 0.29, reflecting mature organic matter in Dishuiquan Formation, while the  $T_{max}$  value indicates an early mature to mature thermal stage for these mudstone samples. The maturity estimates suggested by the  $T_{max}$  and PI values are slightly inconsistent, likely due to a low degree of petroleum generation, which can affect the Rock-Eval pyrolysis data (Lo and Cardott, 1995).

Biomarker parameters supplement our understanding of the thermal maturity of the source rocks. The ratio of 22S/(22S + 22R) for the  $17\beta,21\alpha(\text{H})-\text{C}_{31}$  hopanes is in the range of 0.54–0.58 (Table 4), whereas the average of 22S/(22S + 22R) for the  $17\beta,21\alpha(\text{H})-\text{C}_{32}$  hopanes is 0.59. These ratios indicate an equilibrium value of 0.5–0.6%  $R_f$  (Mackenzie and Maxwell, 1981). The isosterane content is primarily related to maturity, which transforms the biologic  $\alpha\alpha\alpha$  forms (normal steranes) into  $\alpha\beta\beta$  forms (Mackenzie and McKenzie, 1983; Seifert and Moldowan, 1986; Spiro et al., 1988; Ten Haven et al., 1986; Waples and Machihara, 1991). The values of 20S/(20S + 20R) and  $\alpha\beta\beta$ /( $\alpha\beta\beta$  +  $\alpha\alpha\alpha$ ) of the  $C_{29}$  steranes show a similar average of 0.42 in

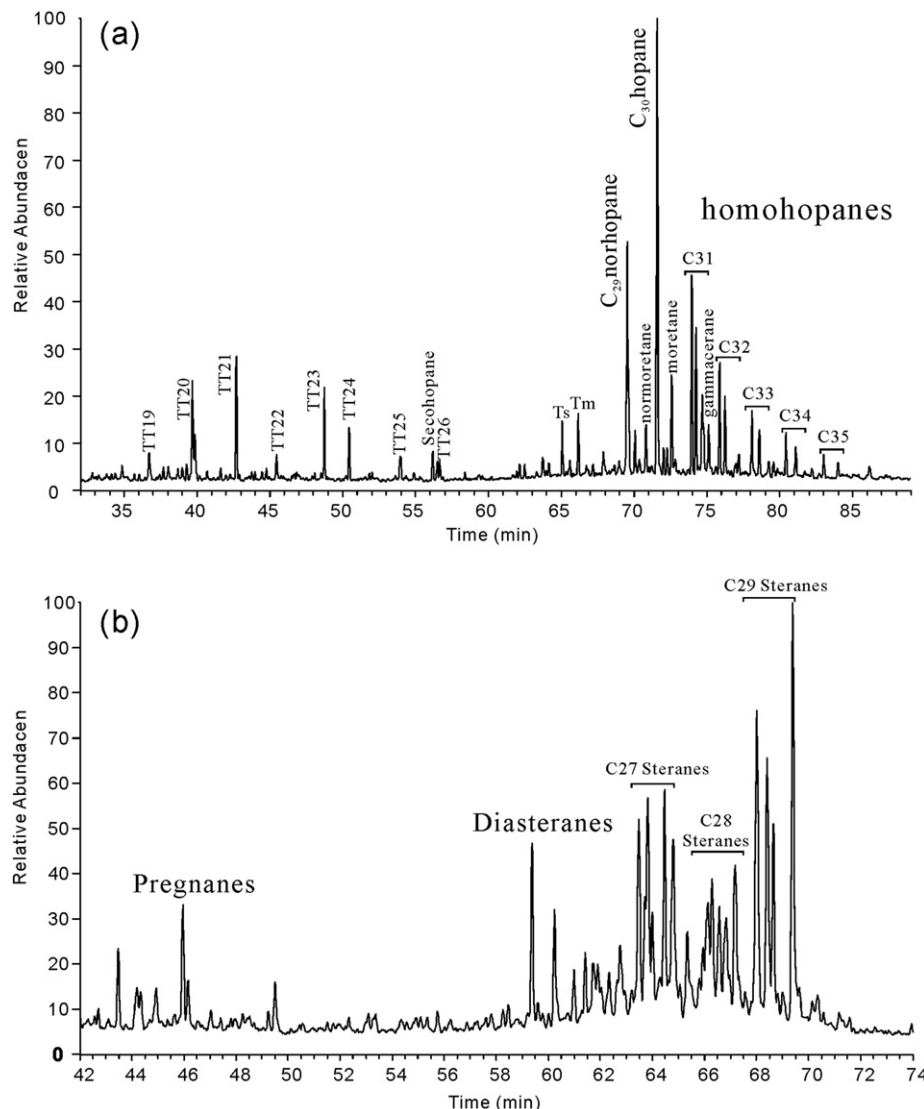


Fig. 7. (a)  $m/z$  191 mass chromatograms of the Dishuiquan Formation mudstone (CC-10), (b)  $m/z$  217 mass chromatograms of the Dishuiquan Formation mudstone (CC-10).

the mudstones from the C-2 well, and equilibrium value of 0.6%  $R_r$  has been attained. Therefore, based on the Rock-Eval, 22S/(22S + 22R) hopanoids, 20S/(20S + 20R) and  $\alpha\beta\beta/(\alpha\beta\beta + \alpha\alpha\alpha)$  of the  $C_{29}$  steranes ratio data, all the samples exhibit an early mature to mature thermal stage.

## 5.2. Organic matter source input and depositional environments

Amorphous sapropelic and humic organic matter are predominant (>65%) in all the samples. The amorphous humic OM is more abundant than the amorphous sapropelic OM, except in sample C-41, which contains 40% amorphous sapropelic OM and 35% amorphous humic OM. Amorphous humic materials were probably formed by the biodegradation of land plants (Styan and Bustin, 1983), and amorphous sapropelic matter is generally related to algal or bacterial sources (Schnyder et al., 2009; Tyson, 1995). The proportions of amorphous sapropelic and humic organic matter reveal a high terrestrial OM contribution in the organic matter of the lower Carboniferous Dishuiquan Formation.

The values of CPI<sub>1</sub> and CPI<sub>2</sub> are 0.94–1.36 and n.d.–3.12, respectively, which indicate that odd-numbered n-alkanes are dominant over even-numbered n-alkanes. The Alkterr exhibits the opposite tendency of  $\sum C_{21-}/\sum C_{22+}$ , which suggests that the organic matter from in situ algae sources gradually decreases in the later periods of the Dishuiquan

Formation. The low Alkterr values can be attributed to three factors: a relatively low contribution of terrestrial organic matter, the fact that terrestrial plants during the early Carboniferous had not evolved into “real” higher plants and the possibility that these early terrestrial plants may also have lacked long-chain n-alkanes. Similar n-alkanes were also detected in Carboniferous coals from the Ruhr Basin, western Germany, which exhibit high ratio of n-C<sub>17</sub>/n-C<sub>27</sub> (Böcker et al., 2013).

Ratios of Pr/Ph that are <1.0 indicate anaerobic conditions during early diagenesis (Damsté and Leeuw, 1987; Risatti et al., 1984). However, Pr/Ph ratios are known to be affected by maturation (Radke et al., 1986; Tissot and Welte, 1984) and by differences in the precursors for acyclic isoprenoids (Brocks et al., 2005; Goossens et al., 1984; Mackenzie et al., 1980; Rontani et al., 1990; Volkman et al., 1992). However, (Peters et al., 2005) argued that Pr/Ph values <0.6 indicate anoxic, commonly hypersaline or carbonate environments, whereas Pr/Ph values >3.0 are typical of terrigenous OM input under oxidative conditions for rocks within the oil-generation window. Given the early mature to mature thermal stage of these rocks, the influence of thermal stress on Pr/Ph ratios can be ruled out. The ratio of Pr to Ph in the samples ranges from 0.77 to 1.76, with an average of 1.24, indicating that dysoxic conditions were present during the deposition of the Dishuiquan Formation. Peters et al. (2005) defined different fields in the plot of Pr/n-C<sub>17</sub> vs. Ph/n-C<sub>18</sub>: Type III, Type II and mixed (Type II/III) domains. The C-2 samples fall into the

**Table 4**

The hopanoid parameters calculated from m/z 191 mass chromatograms of samples from Dishuiquan Formation.

Sample no.	C31 $\alpha\beta$ -22S/(S + R)	C32 $\alpha\beta$ -22S/(S + R)	Gammacerane index <sup>a</sup>	Ts/Tm	C <sub>29</sub> /C <sub>30</sub>	C <sub>35</sub> /C <sub>34</sub>
CC-2	0.58	0.60	0.60	1.09	0.53	0.44
CC-3	0.57	0.60	0.57	0.92	0.60	0.43
CC-4	0.58	0.58	0.31	0.67	0.53	0.46
CC-5	0.58	0.58	0.42	1.05	0.61	0.42
CC-9	0.54	0.60	0.89	0.89	0.55	0.52
CC-10	0.58	0.59	0.46	0.89	0.51	0.53
CC-11	0.57	0.60	0.51	1.06	0.52	0.45
CC-12	0.58	0.59	0.43	0.84	0.52	0.46
CC-13	0.57	0.59	0.40	0.93	0.54	0.42
CC-14	0.57	0.58	0.48	0.82	0.50	0.51
CC-15	0.58	0.60	0.32	0.87	0.66	0.42
CC-16	0.58	0.59	0.53	0.98	0.53	0.40
CC-17	0.55	0.58	0.78	1.12	0.48	0.51
CC-18	0.57	0.59	0.64	0.93	0.50	0.44
CC-19	0.57	0.59	0.60	0.76	0.56	0.46
CC-20	0.56	0.58	0.62	0.66	0.51	0.53
CC-21	0.57	0.60	0.54	0.82	0.60	0.43
CC-22	0.57	0.59	0.54	0.84	0.56	0.44
CC-23	0.57	0.59	0.50	0.68	0.53	0.45
CC-24	0.56	0.59	0.56	0.77	0.57	0.47
CC-25	0.58	0.58	0.44	0.62	0.59	0.44
CC-26	0.56	0.58	0.87	0.94	0.45	0.59
CC-27	0.57	0.60	0.82	0.99	0.52	0.48
CC-28	0.58	0.58	0.67	0.71	0.53	0.50
CC-29	0.57	0.61	0.74	0.92	0.54	0.44
CC-30	0.57	0.59	0.68	0.81	0.56	0.45
CC-31	0.56	0.59	0.83	0.96	0.47	0.57
CC-32	0.57	0.60	0.77	0.97	0.55	0.47
CC-33	0.56	0.59	0.79	0.95	0.47	0.55
CC-34	0.55	0.58	0.88	1.07	0.45	0.52
CC-35	0.56	0.60	0.94	1.13	0.45	0.56
CC-36	0.56	0.59	0.84	1.00	0.48	0.51
CC-37	0.56	0.59	0.77	0.85	0.57	0.51
CC-38	0.55	0.59	1.00	1.51	0.45	0.54
CC-40	0.57	0.60	0.89	1.25	0.50	0.52
CC-41	0.57	0.61	0.92	1.50	0.47	0.51
CC-42	0.58	0.61	1.01	1.98	0.49	0.54
CC-43	0.58	0.61	0.98	1.66	0.51	0.46
CC-44	0.55	0.57	1.05	1.91	0.40	0.64
CC-45	0.57	0.58	0.85	1.69	0.45	0.46
CC-46	0.55	0.59	1.00	1.71	0.38	0.57
CC-48	0.56	0.59	1.04	1.74	0.41	0.66
CC-49	0.58	0.59	0.56	1.04	0.58	0.35

<sup>a</sup> Gammacerane index = 2 × gammacerane/(S + R)-C<sub>30</sub> hopanes.

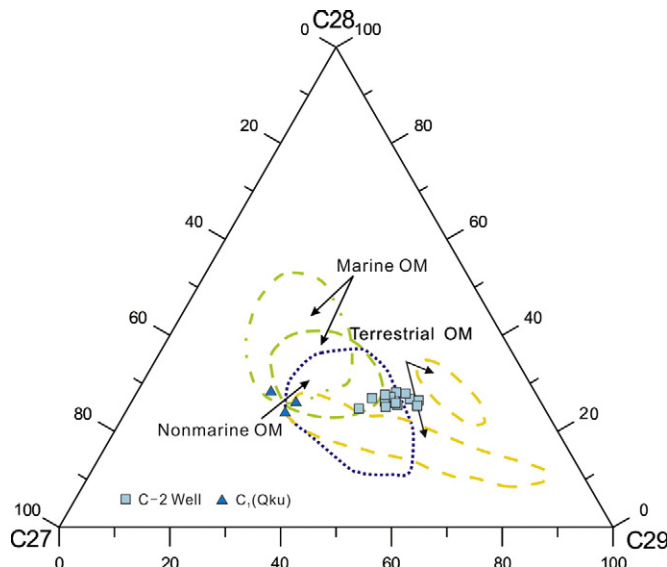


**Fig. 8.** Distribution diagrams of  $C_{27}$ ,  $C_{28}$ , and  $C_{29}$   $5\alpha,14\alpha,17\alpha(H)20R$  sterane of the Dishuiquan samples and Qiakuerter Outcrop (Qku) of Nanmingshui Formation (Qin et al., 2008), according to Peter (1986).

mixed (Type II/III) domain (Fig. 5), which can be explained by the presence of both algae and higher plants.

$\beta$ -Carotane is the most prominent compound of the carotenoid carbon skeleton preserved in lacustrine and highly restricted marine depositional settings (Peters et al., 2005). This aromatic carotenoid was first identified in the Green River Shale (Murphy et al., 1967).  $\beta$ -Carotane was later found in numerous sedimentary rocks and crude oils (Bechtel et al., 2012; Brocks and Schaeffer, 2008; Casilli et al., 2014; Jiang and Fowler, 1986; Sousa Júnior et al., 2013). The compound is also reported in the upper Permian oil shale from Southern Junggar (Carroll, 1998). The ratio of  $\beta$ -carotane and the sum of n-alkanes ( $\beta$ -carotane/ $\Sigma C_{12-35}$ ) is in the range of n.d.–4.48%, and the values decrease upward. The abundance of  $\beta$ -carotane indicates highly reducing conditions involving salinity stratification during the early Carboniferous. The high concentrations of the molecule in the mudstone from the C-2 well were generated by a stratified water column that was characterized by low Pr/Ph ratios (Fig. 6, Table 3). The effect of salinity stratification on the preservation of carotenoids is clearly demonstrated by the negative correlation between the value of  $\beta$ -carotane/ $\Sigma C_{12-35}$  and the Pr/Ph ratio (Fig. 6). This relationship indicates that terrestrial fresh water was continuously added to the restricted water column.

The values of  $C_{35}/C_{34}$  22S homohopanes and norhopane/hopane ( $C_{29}/C_{30}$ ) can be used to define source facies (Peters et al., 2005). The

**Table 5**

The sterane parameters calculated from  $m/z$  217 mass chromatograms of samples from Dishuiquan Formation.

Sample no.	$C_{29}\alpha\alpha\alpha-20S/20(S + R)$	$C_{29}\alpha\beta\beta/(\alpha\beta\beta + \alpha\alpha\alpha)$	$C_{27}\alpha\alpha\alpha20R$	$C_{28}\alpha\alpha\alpha20R$	$C_{29}\alpha\alpha\alpha20R$
CC-2	0.42	0.39	27.13	23.83	49.04
CC-3	0.41	0.37	22.98	25.53	51.49
CC-4	0.43	0.37	24.43	19.89	55.68
CC-5	0.43	0.39	29.78	22.13	48.09
CC-9	0.44	0.49	17.34	28.64	54.02
CC-10	0.42	0.38	28.12	18.60	53.29
CC-11	0.43	0.40	29.08	18.54	52.39
CC-12	0.43	0.40	26.02	18.32	55.66
CC-13	0.43	0.39	27.78	19.05	53.17
CC-14	0.42	0.39	24.36	19.50	56.14
CC-15	0.44	0.41	28.98	19.34	51.68
CC-16	0.43	0.40	26.31	22.78	50.91
CC-17	0.43	0.42	20.16	26.75	53.09
CC-18	0.42	0.41	24.92	23.22	51.86
CC-19	0.44	0.41	24.69	24.00	51.31
CC-20	0.41	0.41	21.42	23.48	55.10
CC-21	0.43	0.41	25.95	23.69	50.37
CC-22	0.43	0.39	26.95	23.32	49.73
CC-23	0.41	0.38	25.63	22.39	51.98
CC-24	0.43	0.41	25.67	24.05	50.28
CC-25	0.43	0.38	28.21	22.44	49.35
CC-26	0.41	0.44	21.28	26.58	52.14
CC-27	0.43	0.42	26.37	25.76	47.88
CC-28	0.42	0.41	24.90	23.73	51.37
CC-29	0.42	0.43	26.49	25.19	48.32
CC-30	0.42	0.42	26.96	24.34	48.69
CC-31	0.41	0.42	24.37	25.50	50.13
CC-32	0.42	0.43	25.76	25.61	48.63
CC-33	0.42	0.42	23.44	25.73	50.83
CC-34	0.42	0.41	21.89	27.31	50.81
CC-35	0.41	0.43	23.59	26.10	50.31
CC-36	0.41	0.43	23.06	25.98	50.96
CC-37	0.44	0.42	29.92	24.04	46.04
CC-38	0.42	0.44	23.99	27.06	48.96
CC-40	0.42	0.45	25.31	26.49	48.20
CC-41	0.42	0.44	24.82	26.76	48.42
CC-42	0.44	0.45	26.92	27.10	45.98
CC-43	0.43	0.44	26.22	26.57	47.21
CC-44	0.39	0.39	20.73	25.07	54.20
CC-45	0.43	0.43	28.07	25.36	46.57
CC-46	0.39	0.42	20.59	24.97	54.44
CC-48	0.42	0.45	23.62	27.34	49.04
CC-49	0.43	0.44	25.06	23.92	51.01

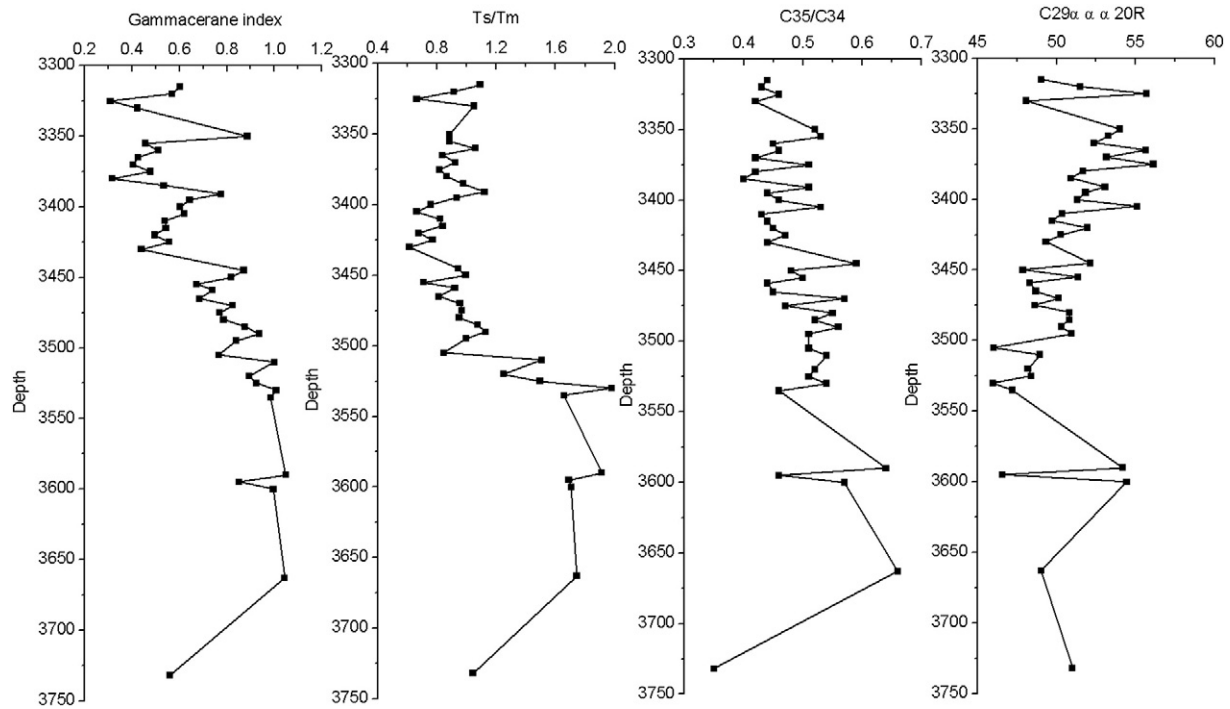


**Fig. 9.** Profile for parameters from hopanoids and steranes of samples from the Dishuiquan Formation.

C-2 samples exhibit averages of 0.49 and 0.52 for  $C_{35}/C_{34}$  and  $C_{29}/C_{30}$ , respectively. The low values for  $C_{35}/C_{34}$  and  $C_{29}/C_{30}$  indicate major terrestrial organic matter contributions in the mudstones during the early Carboniferous. The upward-decreasing values represent the increasing input of terrestrial organic matter (Fig. 8), which agrees with the tendency from  $Alk_{terr}$  values from the n-alkanes.

Gammacerane was detected in all the samples from the C-2 well in Eastern Junggar. The origin of gammacerane is uncertain, but it may form via the reduction of tetrahymanol associated with the presence of planktonic bacteriovorus ciliates (Grice et al., 1998). High tetrahymanol abundance occurs in sediments from the eutrophic Lake Lugano (Bechtel and Schubert, 2009). The gammacerane index calculated from the ratio of  $2 \times$  gammacerane/(S + R)- $C_{30}$  hopanes is in the range of 0.62 to 1.89 (Table 4), and the values decrease upward. The compound 18  $\alpha$ (H)-22,29,30-trisnorhopane (Ts) is generally considered to be more thermally stable than 17  $\alpha$ (H)-22,29,30-trisnorhopane (Tm). However, the ratio of Ts to Tm is more related to

the salinity and redox conditions in the immature-early maturity thermal stages, and high Ts/Tm values reflect a highly saline reducing environment (Peters and Moldowan, 1993). The Ts/Tm values range from 0.62 to 1.98, a range similar to the gammacerane index ( $R^2 = 0.58$ ) (Fig. 8). These values indicate that the salinity and redox conditions were an important factor in the distribution of Ts and Tm.

The 5 $\alpha$ ,14 $\alpha$ ,17 $\alpha$ (H) steranes, dominated by the 5 $\alpha$ ,14 $\alpha$ ,17 $\alpha$ (H) isomers, are present in the  $C_{27}$ - $C_{29}$  range (Fig. 7b), consistent with the low maturity-early maturity of the samples. Algae are the predominant primary producers of  $C_{27}$  sterols, whereas  $C_{29}$  steranes are commonly associated with higher plants (Volkman, 1986). However, microalgae or cyanobacteria can also be important sources of  $C_{29}$  sterols (Volkman, 1986; Volkman et al., 1992). The  $C_{27}$ ,  $C_{28}$ , and  $C_{29}$  distributions imply that there are greater contributions from terrestrial higher plants than marine algae in the Dishuiquan Formation mudstone (Fig. 8). The upward increase in the  $C_{29}$  steranes indicates that the increasing contribution occurred during the later stages of the early

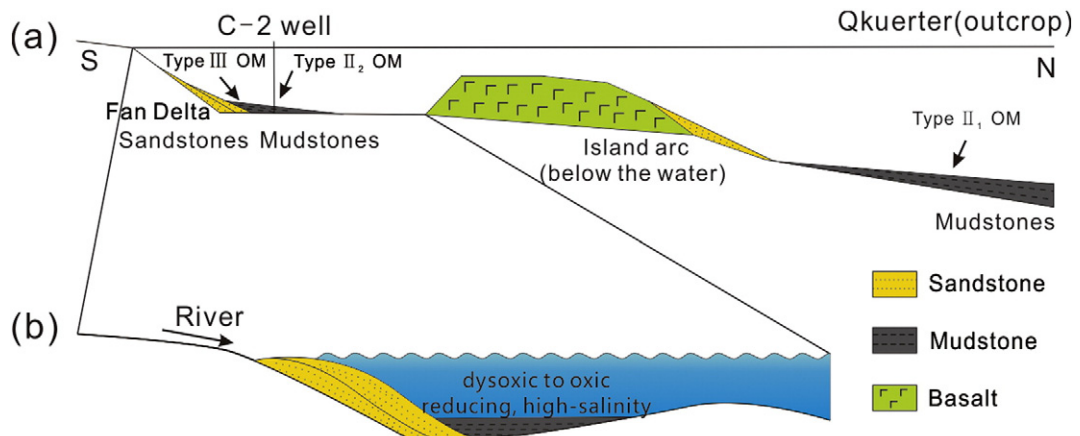


**Fig. 10.** Paleogeographic sections (a) and paleoenvironment (b) during Early Carboniferous.

Carboniferous, which is consistent with the previously discussed data. The abundance of C<sub>29</sub> steranes in samples CC-44, -46, and -49 is likely due to terrigenous plant debris transported by river currents (Fig. 9).

Carbon isotopic ratios are useful for distinguishing between marine and continental plant sources of sedimentary organic matter and for identifying organic matter from different types of land plants (Meyers, 1997). The  $\delta^{13}\text{C}$  values for kerogen from all the selected samples show a light carbon isotopic composition within the C3 plant range (Lichtfouse et al., 1994; Meyers and Ishiwatari, 1993; Meyers and Lallier-Vergès, 1999; O'Leary, 1988). However, the stable carbon isotope values of kerogen and chloroform extract are higher than the  $\delta^{13}\text{C}$  values produced by typical terrestrial plants deposited in modern lakes or marginal seas. Whereas no evidences show that C4 plants occurred on Earth before Oligocene (Nelson et al., 2014), this pattern suggests that the former terrestrial plants, which colonized dry areas such as alluvial plains and evaporitic sabkhas, had not evolved into the true terrestrial plants using a modern C3 photosynthetic pathway. The distribution of carbon isotopic compositions also agrees with the Alkterr estimates calculated using n-alkanes, which are produced by certain types of terrestrial plants that originated from the paleomarine environment in the early Paleozoic.

This study used the maceral composition, molecular geochemistry and carbon isotopic composition of kerogen to interpret the paleoenvironment during the lower Carboniferous succession in Eastern Junggar. The mudstone samples from the C-2 well are characterized by a mixed organic matter (Type II/III kerogen) assemblage with a relatively high percentage of terrigenous organic matter and a low to intermediate percentage of algal and planktonic organic matter. The low to intermediate values of Pr/Ph and the high abundances of  $\beta$ -carotane and gammacerane indicate a dysoxic to reducing, high-salinity water column during the deposition of the Dishuiquan Formation. Moreover, the relative content of C<sub>29</sub> steranes in the Qiakuerter Outcrop (Qku) (Qin et al., 2008) of the Nanmingshui Formation (equivalent to the Dishuiquan Formation) is lower than in the samples from the C-2 well, which implies that the C-2 well is located in a more proximal position (Fig. 10). In general, such an organic matter assemblage and hydrologic condition are considered to indicate a restricted, semi-closed shallow marine depositional environment into which terrigenous organic matter was transported via rivers from the nearby island arc (Fig. 10).

The increase in terrigenous organic matter with decreasing salinity and oxidation in the sedimentary environment is noteworthy. These trends in the proportion of terrigenous organic matter and the salinity and oxidation conditions of the water column may have been affected by two factors: a continuous regression of the restricted, semi-closed marine depositional environment or a warm, wet climate that generated a continuous fluvial input of terrigenous plant debris and fresh water. In summary, a dysoxic, reducing shallow marine environment may have been present during the studied interval in Eastern Junggar. The Paleo-Junggar Ocean had not closed completely in the early Carboniferous; however, the ocean had already experienced a regression, which continued until the ocean's closure.

## 6. Conclusions

A detailed organofacies and organic geochemical study of 49 Dishuiquan Formation mudstone samples from the C-2 well, Eastern Junggar, was performed. This study describes the paleoenvironment and paleoclimate of the region in the early Carboniferous and the source potential of these mudstones. The following conclusions have been found.

1. The TOC and Rock-Eval results suggest a fair to good organic richness in the Dishuiquan mudstone samples in the C-2 well. The samples are characterized by Type II–III kerogen in the HI vs.  $T_{\max}$  diagram, and substantial amounts of amorphous humic organic matter were detected.

2. The values of 22S/(22S + 22R) of hopanoids, 20S/(20S + 20R) and  $\alpha\beta/(\alpha\beta\beta + \alpha\alpha\alpha)$  of C<sub>29</sub> steranes indicate an early mature to mature state for all the samples from the Dishuiquan Formation. However, the Dishuiquan Formation was buried to a greater depth in the Eastern Junggar Basin, and that portion may act as a petroleum source rock for the overlying strata.
3. The maceral composition, molecular geochemistry and carbon isotopic composition of kerogen reveal that all the mudstone samples are characterized by a mixed organic matter assemblage with a relatively higher percentage of terrigenous organic matter and low to intermediate percentages of algal and planktonic organic matter. The low to intermediate values of Pr/Ph and the high abundances of  $\beta$ -carotane and gammacerane indicate that a reducing, high-salinity water column was present during the deposition of the Dishuiquan Formation.
4. Numerous parameters derived from organic geochemical analyses demonstrate that the terrigenous organic matter percentage increases with decreasing salinity and oxidation in the sedimentary environment. This study concludes that a warm, wet climate provided a continuous fluvial input of terrigenous plant debris and fresh water to a restricted, semi-closed marine depositional environment during the early Carboniferous.

## Acknowledgments

The Xinjiang Oilfield Company kindly supplied borehole core samples of the Carboniferous in the Junggar Basin. We gratefully acknowledge two anonymous referees for their reviews. This research was financially supported by the National Science and Technology Major Project (2011ZX05008-003) and the Key Laboratory Project of Gansu Province (Grant No. 1309RTSA041).

## References

- Bechtel, A., Schubert, C.J., 2009. A biogeochemical study of sediments from the eutrophic Lake Lugano and the oligotrophic Lake Brienz, Switzerland. *Org. Geochem.* 40, 1100–1114.
- Bechtel, A., Jia, J., Strobl, S.A.I., Sachsenhofer, R.F., Liu, Z., Grätzer, R., Püttmann, W., 2012. Palaeoenvironmental conditions during deposition of the Upper Cretaceous oil shale sequences in the Songliao Basin (NE China): implications from geochemical analysis. *Org. Geochem.* 46, 76–95.
- Böcker, J., Little, R., Hartkopf-Fröder, C., Jasper, K., Schwarzbauer, J., 2013. Organic geochemistry of Duckmantian (Pennsylvanian) coals from the Ruhr Basin, western Germany. *Int. J. Coal Geol.* 107, 112–126.
- Bray, E., Evans, E., 1961. Distribution of paraffins as a clue to recognition of source beds. *Geochim. Cosmochim. Acta* 22, 2–15.
- Brocks, J.J., Schaeffer, P., 2008. Okenane, a biomarker for purple sulfur bacteria (*Chromatiaceae*), and other new carotenoid derivatives from the 1640 Ma Barney Creek Formation. *Geochim. Cosmochim. Acta* 72, 1396–1414.
- Brocks, J.J., Love, G.D., Summons, R.E., Knoll, A.H., Logan, G.A., Bowden, S.A., 2005. Biomarker evidence for green and purple sulphur bacteria in a stratified Palaeoproterozoic sea. *Nature* 437, 866–870.
- Cai, K., Sun, M., Yuan, C., Xiao, W., Zhao, G., Long, X., Wu, F., 2012. Carboniferous mantle-derived felsic intrusion in the Chinese Altai, NW China: implications for geodynamic change of the accretionary orogenic belt. *Gondwana Res.* 22, 681–698.
- Carroll, A.R., 1998. Upper Permian lacustrine organic facies evolution, Southern Junggar Basin, NW China. *Org. Geochem.* 28, 649–667.
- Casilli, A., Silva, R.C., Laakja, J., Oliveira, C.J.F., Ferreira, A.A., Loureiro, M.R.B., Azevedo, D.A., Aquino Neto, F.R., 2014. High resolution molecular organic geochemistry assessment of Brazilian lacustrine crude oils. *Org. Geochem.* 68, 61–70.
- Chen, B., Jahn, B.-m., 2004. Genesis of post-collisional granitoids and basement nature of the Junggar Terrane, NW China: Nd–Sr isotope and trace element evidence. *J. Asian Earth Sci.* 23, 691–703.
- Connan, J., Cassou, A., 1980. Properties of gases and petroleum liquids derived from terrestrial kerogen at various maturation levels. *Geochim. Cosmochim. Acta* 44, 1–23.
- Damsté, T.H., Leeuw, J., 1987. Restricted utility of the pristine/phytane ratio as a palaeoenvironmental indicator. *Nature* 330, 641–643.
- Espitalié, J., Senga Makadi, K., Trichet, J., 1984. Role of the mineral matrix during kerogen pyrolysis. *Org. Geochem.* 6, 365–382.
- Espitalié, J., 1986. Use of  $T_{\max}$  as a maturation index for different types of organic matter. Comparison with vitrinite reflectance. Thermal modelling in sedimentary basins. *Ed. Technip Paris*, pp. 475–496.
- Fu, X., Wang, J., Zeng, Y., Li, Z., Wang, Z., 2009. Geochemical and palynological investigation of the Shengli River marine oil shale (China): implications for paleoenvironment and paleoclimate. *Int. J. Coal Geol.* 78, 217–224.

- Goossens, H., De Leeuw, J., Schenck, P., Brassell, S., 1984. Tocopherols as likely precursors of pristane in ancient sediments and crude oils. *Nature* 312, 440–442.
- Grice, K., Schouten, S., Nissenbaum, A., Charach, J., Sinnonghe Damsté, J.S., 1998. A remarkable paradox: sulfurised freshwater algal (*Botryococcus braunii*) lipids in an ancient hypersaline euxinic ecosystem. *Org. Geochem.* 28, 195–216.
- Han, B.-F., He, G.-Q., Wang, X.-C., Guo, Z.-J., 2011. Late Carboniferous collision between the Tarim and Kazakhstan–Yili terranes in the western segment of the South Tian Shan Orogen, Central Asia, and implications for the Northern Xinjiang, western China. *Earth Sci. Rev.* 109, 74–93.
- Han, Z., Xu, M., Li, Y., Wei, Y., Wang, C., 2014. Paleocene-Eocene potential source rocks in the Avengco Basin, Tibet: organic geochemical characteristics and their implication for the paleoenvironment. *J. Asian Earth Sci.* 93, 60–73.
- He, D., Chen, X., Kuang, J., Yuan, H., Fan, C., Tang, Y., Wu, X., 2010. Distribution of Carboniferous source rocks and petroleum systems in the Junggar Basin. *Pet. Explor. Dev.* 37, 397–408.
- He, D.-F., Li, D., Fan, C., Yang, X.-F., 2013. Geochronology, geochemistry and tectonostratigraphy of Carboniferous strata of the deepest Well Moshen-1 in the Junggar Basin, northwest China: insights into the continental growth of Central Asia. *Gondwana Res.* 24, 560–577.
- Hunt, J.M., 1996. *Petroleum Geochemistry and Geology*.
- Jian, P., Liu, D., Zhang, Q., Zhang, F., Shi, Y., Shi, G., Zhang, L., 2003. SHRIMP dating of ophiolite and leucocratic rocks within ophiolite. *Earth Sci. Front.* 10, 18.
- Jiang, Z.S., Fowler, M.G., 1986. Carotenoid-derived alkanes in oils from northwestern China. *Org. Geochem.* 10, 831–839.
- Langford, F., Blanc-Valleron, M.-M., 1990. Interpreting Rock-Eval pyrolysis data using graphs of pyrolyzable hydrocarbons vs. total organic carbon (1). *AAPG Bull.* 74, 799–804.
- Li, D., He, D.-F., Santosh, M., Tang, J.-y., 2014. Petrogenesis of Late Paleozoic volcanics from the Zhaheba depression, East Junggar: insights into collisional event in an accretionary orogen of Central Asia. *Lithos* 184–187, 167–193.
- Lichtfouse, E., Elbissar, B., Balesdent, J., Mariotti, A., Bardoux, G., 1994. Isotope and molecular evidence for direct input of maize leaf wax alkanes into crop soils. *Org. Geochem.* 22, 349–351.
- Littke, R., Urai, J.L., Uffmann, A.K., Risvanis, F., 2012. Reflectance of dispersed vitrinite in Palaeozoic rocks with and without cleavage: implications for burial and thermal history modeling in the Devonian of Rursee area, northern Rhenish Massif, Germany. *Int. J. Coal Geol.* 89, 41–50.
- Liu, W., Liu, X.-J., Liu, L.-J., 2013. Underplating generated A- and I-type granitoids of the East Junggar from the lower and the upper oceanic crust with mixing of mafic magma: insights from integrated zircon U-Pb ages, petrography, geochemistry and Nd-Sr-Hf isotopes. *Lithos* 179, 293–319.
- Lo, H.B., Cardott, B.J., 1995. Detection of natural weathering of Upper McAlester coal and Woodford Shale, Oklahoma, U.S.A. *Org. Geochem.* 22, 73–83.
- Mackenzie, A., Maxwell, J., 1981. Assessment of thermal maturation in sedimentary rocks by molecular measurements. *Organic Maturation Studies and Fossil Fuel Exploration*. Academic Press, London, pp. 239–254.
- Mackenzie, A., McKenzie, D., 1983. Isomerization and aromatization of hydrocarbons in sedimentary basins formed by extension. *Geol. Mag.* 120, 417–470.
- Mackenzie, A., Patience, R., Maxwell, J., Vandebroucke, M., Durand, B., 1980. Molecular parameters of maturation in the Toarcian shales, Paris Basin, France—I. Changes in the configurations of acyclic isoprenoid alkanes, steranes and triterpanes. *Geochim. Cosmochim. Acta* 44, 1709–1721.
- Meyers, P.A., 1997. Organic geochemical proxies of paleoceanographic, paleolimnologic, and paleoclimatic processes. *Org. Geochem.* 27, 213–250.
- Meyers, P.A., Ishiwatari, R., 1993. Lacustrine organic geochemistry—an overview of indicators of organic matter sources and diagenesis in lake sediments. *Org. Geochem.* 20, 867–900.
- Meyers, P.A., Lallier-Vergès, E., 1999. Lacustrine sedimentary organic matter records of Late Quaternary paleoclimates. *J. Paleolimnol.* 21, 345–372.
- Murphy, S.M.T., McCormick, A., Eglington, G., 1967. Perhydro- $\beta$ -carotene in the Green River Shale. *Science* 157, 1040–1042.
- Nelson, D.M., Urban, M.A., Hu, F.S., 2014. Spatiotemporal variation in the origin of C4 grasses:  $\delta^{13}\text{C}$  analysis of grass pollen from the southeastern United States. *Palaeogeogr. Palaeoclimatol. Palaeoecol.* 396, 227–231.
- O'Leary, M.H., 1988. Carbon isotopes in photosynthesis. *Bioscience* 328–336.
- Peter, K.E., 1986. Guidelines for evaluating petroleum source rock using programmed pyrolysis. *AAPG Bull.* 70, 12.
- Peters, K.E., Moldowan, J.M., 1993. The biomarker guide: interpreting molecular fossils in petroleum and ancient sediments.
- Peters, K.E., Walters, C.C., Moldowan, J.M., 2005. *The Biomarker Guide: Biomarkers and Isotopes in the Environment and Human History*. Cambridge University Press.
- Petersen, H.I., Tru, V., Nielsen, L.H., Duc, N.A., Nytoft, H.P., 2005. Source rock properties of lacustrine mudstones and coals (Oligocene Dong Ho Formation), onshore Song Hong Basin, Northern Vietnam. *J. Pet. Geol.* 28, 19–38.
- Qin, L., Zhang, Z., Liu, H., 2008. Geochemical characteristics of lower Carboniferous Nanmingshui Formation source rock and their geological implication, Qiakuerte Prairie, northeastern Junggar basin. *Nat. Gas Geosci.* 19, 761–769.
- Radke, M., Welte, D., Willsch, H., 1986. Maturity parameters based on aromatic hydrocarbons: influence of the organic matter type. *Org. Geochem.* 10, 51–63.
- Risatti, J., Rowland, S., Yon, D., Maxwell, J., 1984. Stereochemical studies of acyclic isoprenoids—XII. Lipids of methanogenic bacteria and possible contributions to sediments. *Org. Geochem.* 6, 93–104.
- Rontani, J., Combe, I., Giral, P.-P., 1990. Abiotic degradation of free phytol in the water column: a new pathway for the production of acyclic isoprenoids in the marine environment. *Geochim. Cosmochim. Acta* 54, 1307–1313.
- Sachse, V.F., Little, R., Jabour, H., Schümann, T., Kluth, O., 2012. Late Cretaceous (Late Turonian, Coniacian and Santonian) petroleum source rocks as part of an OAE, Tarfaya Basin, Morocco. *Mar. Pet. Geol.* 29, 35–49.
- Schnyder, J., Dejax, J., Keppens, E., Nguyen Tu, T.T., Spagna, P., Boulila, S., Galbrun, B., Ribouleau, A., Tshibangu, J.-P., Yans, J., 2009. An Early Cretaceous lacustrine record: organic matter and organic carbon isotopes at Bernissart (Mons Basin, Belgium). *Palaeogeogr. Palaeoclimatol. Palaeoecol.* 281, 79–91.
- Seifert, W., Moldowan, J., 1986. Use of biological markers in petroleum exploration. *Methods Geochem. Geophys.* 24, 261–290.
- Song, Z., Qin, Y., George, S.C., Wang, L., Guo, J., Feng, Z., 2013. A biomarker study of depositional paleoenvironments and source inputs for the massive formation of Upper Cretaceous lacustrine source rocks in the Songliao Basin, China. *Palaeogeogr. Palaeoclimatol. Palaeoecol.* 385, 137–151.
- Sousa Júnior, G.R., Santos, A.L.S., de Lima, S.G., Lopes, J.A.D., Reis, F.A.M., Santos Neto, E.V., Chang, H.K., 2013. Evidence for euphotic zone anoxia during the deposition of Aptian source rocks based on aryl isoprenoids in petroleum, Sergipe–Alagoas Basin, north-eastern Brazil. *Org. Geochem.* 63, 94–104.
- Spiro, R., Wolf, R., Fejer, B.G., 1988. Penetrating of high-latitude-electric-field effects to low latitudes during SUNDIAL 1984. *Ann. Geophys.* 39–49.
- Styan, W.t., Bustin, R., 1983. Petrography of some Fraser river delta peat deposits: coal maceral and microlithotype precursors in temperate-climate peats. *Int. J. Coal Geol.* 2, 321–370.
- Su, Y., Zheng, J., Griffin, W.I., Zhao, J., Tang, H., Ma, Q., Lin, X., 2012. Geochemistry and geochronology of Carboniferous volcanic rocks in the eastern Junggar terrane, NW China: implication for a tectonic transition. *Gondwana Res.* 22, 1009–1029.
- Tang, H., Su, Y., Liu, C., Hou, G., Wang, Y., 2007. Zircon U-Pb age of the plagiogranite in Kalamaili belt, northern Xinjiang and its tectonic implications. *Geotecton. Metallog.* 31, 8.
- Tao, H., Sun, S., Wang, Q., Yang, X., Jiang, L., 2014. Petrography and geochemistry of lower carboniferous greywacke and mudstones in Northeast Junggar, China: implications for provenance, source weathering, and tectonic setting. *J. Asian Earth Sci.* 87, 11–25.
- Ten Haven, H., De Leeuw, J., Peakman, T., Maxwell, J., 1986. Anomalies in steroid and hopanoid maturity indices. *Geochim. Cosmochim. Acta* 50, 853–855.
- Tissot, B.P., Welte, D.H., 1984. *Petroleum Formation and Occurrence*.
- Tyson, R.V., 1995. *Sedimentary Organic Matter: Organic Facies and Palynofacies*. Springer.
- Volkman, J.K., 1986. A review of sterol markers for marine and terrigenous organic matter. *Org. Geochem.* 9, 83–99.
- Volkman, J.K., Holdsworth, D.G., Neill, G.P., Bavor Jr., H., 1992. Identification of natural, anthropogenic and petroleum hydrocarbons in aquatic sediments. *Sci. Total Environ.* 112, 203–219.
- Wang, X., Zhao, M., Xiang, B., Da, J., Jiang, Y., Liu, C., 2010. Carboniferous source rocks in the Ludong–Wucaitan area, Junggar Basin, NW China. *Pet. Explor. Dev.* 37, 523–530.
- Wang, L., Wang, C., Li, Y., Zhu, L., Wei, Y., 2011. Sedimentary and organic geochemical investigation of tertiary lacustrine oil shale in the central Tibetan plateau: Palaeolimnological and palaeoclimatic significances. *Int. J. Coal Geol.* 86, 254–265.
- Wang, S., Zou, C., Hou, L., Wei, Y., Luo, X., Guo, Z., 2013. Petroleum geological characteristics of gas accumulation in Carboniferous volcanics and respect for gas exploration, Eastern Junggar Basin. *Earth Sci. Front.* 20, 11.
- Waples, D., Machihara, T., 1991. *Biomarkers for geologist*. American Association of Petroleum Geologists/METHODS in Exploration Series.
- Wilhem, C., Windley, B.F., Stampfli, G.M., 2012. The Altaiids of Central Asia: a tectonic and evolutionary innovative review. *Earth Sci. Rev.* 113, 303–341.
- Xiao, W., Santosh, M., 2014. The western Central Asian Orogenic Belt: a window to accretionary orogenesis and continental growth. *Gondwana Res.* 25, 1429–1444.
- Xiao, W.J., Windley, B.F., Yan, Q.R., Qin, K.Z., Chen, H.L., Yuan, C., Sun, M., Li, J.L., Sun, S., 2006. SHRIMP zircon ages of the Armatai ophiolite in the North Xinjiang area, China, and its tectonic implication. *Acta Geol. Sin.* 80, 6.
- Xiao, W., Huang, B., Han, C., Sun, S., Li, J., 2010. A review of the western part of the Altaiids: a key to understanding the architecture of accretionary orogens. *Gondwana Res.* 18, 253–273.
- Xiao, W., Windley, B.F., Allen, M.B., Han, C., 2013. Paleozoic multiple accretionary and collisional tectonics of the Chinese Tianshan orogenic collage. *Gondwana Res.* 23, 1316–1341.
- Xu, Q.-Q., Ji, J.-Q., Zhao, L., Gong, J.-F., Zhou, J., He, G.-Q., Zhong, D.-L., Wang, J.-D., Griffiths, L., 2013. Tectonic evolution and continental crust growth of Northern Xinjiang in northwestern China: remnant ocean model. *Earth Sci. Rev.* 126, 178–205.
- Yang, G., Li, Y., Wu, H., Zhong, X., Yang, B., Yan, C., Yan, J., Si, G., 2011. Geochronological and geochemical constraints on petrogenesis of the Huangyangshan A-type granite from the East Junggar, Xinjiang, NW China. *J. Asian Earth Sci.* 40, 722–736.
- Yang, G., Li, Y., Santosh, M., Yang, B., Yan, J., Zhang, B., Tong, L., 2012a. Geochronology and geochemistry of basaltic rocks from the Sartuhai ophiolitic mélange, NW China: implications for a Devonian mantle plume within the Junggar Ocean. *J. Asian Earth Sci.* 59, 141–155.
- Yang, X.-F., He, D.-F., Wang, Q.-C., Tang, Y., 2012b. Tectonostratigraphic evolution of the Carboniferous arc-related basin in the East Junggar Basin, northwest China: insights into its link with the subduction process. *Gondwana Res.* 22, 1030–1046.
- Yang, X.-F., He, D.-F., Wang, Q.-C., Tang, Y., Tao, H.-F., Li, D., 2012c. Provenance and tectonic setting of the Carboniferous sedimentary rocks of the East Junggar Basin, China: evidence from geochemistry and U-Pb zircon geochronology. *Gondwana Res.* 22, 567–584.
- Zhang, Y., Gu, Z., 2010. New constraints on formation ages of ophiolites in northern Junggar and comparative study on their connection. *Acta Petrol. Sin.* 26, 10.
- Zhang, Z., Zhou, G., Kusky, T.M., Yan, S., Chen, B., Zhao, L., 2009. Late Paleozoic volcanic record of the Eastern Junggar terrane, Xinjiang, Northwestern China: major and trace element characteristics, Sr-Nd isotopic systematics and implications for tectonic evolution. *Gondwana Res.* 16, 201–215.
- Zou, C., Zhang, G., Zhu, R., Yuan, X., Zhao, X., Hou, L., Wen, B., Wu, X., 2013. Chapter 1 – Exploration History and Features of Volcanic Reservoirs. In: Zou, C., Zhang, G., Zhu, R., Yuan, X., Zhao, X., Hou, L., Wen, B., Wu, X. (Eds.), *Volcanic Reservoirs in Petroleum Exploration*. Elsevier, Boston, pp. 1–10.